



# Respiratory and cardiac motion correction in positron emission tomography using elastic motion approach for simultaneous abdomen and thorax positron emission tomography-magnetic resonance imaging

Adam Farag<sup>1^</sup>, Joshua Schaefferkoetter<sup>2</sup>, Andres Kohan<sup>1</sup>, Inki Hong<sup>2</sup>, Judson Jones<sup>2</sup>, Teodor Stanescu<sup>3</sup>, Kate Hanneman<sup>1</sup>, Gonzalo Sapisochin<sup>4</sup>, Ivan Yeung<sup>3</sup>, Ur Metser<sup>1</sup>, Patrick Veit-Haibach<sup>1</sup>

<sup>1</sup>Joint Department of Medical Imaging, University Health Network, Mount Sinai Hospital and Women's College Hospital, University of Toronto, Toronto, ON, Canada; <sup>2</sup>Siemens Medical Solutions USA, Knoxville, TN, USA; <sup>3</sup>Radiation Medicine Program, Princess Margaret Cancer Centre, University Health Network, Toronto, ON, Canada; <sup>4</sup>Abdominal Transplant & HPB Surgical Oncology, University Health Network, University of Toronto, Toronto, ON, Canada

*Contributions:* (I) Conception and design: J Schaefferkoetter, P Veit-Haibach; (II) Administrative support: None; (III) Provision of study materials or patients: I Hong, J Jones, T Stanescu; (IV) Collection and assembly of data: J Schaefferkoetter, A Kohan; (V) Data analysis and interpretation: A Farag, J Schaefferkoetter, P Veit-Haibach; (VI) Manuscript writing: All authors; (VII) Final approval of manuscript: All authors.

*Correspondence to:* Adam Farag. Joint Department of Medical Imaging, University Health Network, Mount Sinai Hospital and Women's College Hospital, University of Toronto, 610 University Ave., Toronto, ON M5G 2M9, Canada. Email: adam.farag@uhn.ca.

**Background:** Cardiac and respiratory motions in clinical positron emission tomography (PET) are a major contributor to inaccurate PET quantification and lesion characterisation. In this study, an elastic motion-correction (eMOCO) technique based on mass preservation optical flow is adapted and investigated for positron emission tomography-magnetic resonance imaging (PET-MRI) applications.

**Methods:** The eMOCO technique was investigated in a motion management QA phantom and in twenty-four patients who underwent PET-MRI for dedicated liver imaging and nine patients for cardiac PET-MRI evaluation. Acquired data were reconstructed with eMOCO and gated motion correction techniques at cardiac, respiratory and dual gating modes, and compared to static images. Standardized uptake value (SUV), signal-to-noise ratio (SNR) of lesion activities from each gating mode and correction technique were measured and their means/standard deviation (SD) were compared using 2-ways ANOVA analysis and post-hoc Tukey's test.

**Results:** Lesions' SNR are highly recovered from phantom and patient studies. The SD of the SUV resulted from the eMOCO technique was statistically significantly less ( $P < 0.01$ ) than the SD resulted from conventional gated and static SUVs at the liver, lung and heart.

**Conclusions:** The eMOCO technique was successfully implemented in PET-MRI in a clinical setting and produced the lowest SD compared to gated and static images, and hence provided the least noisy PET images. Therefore, the eMOCO technique can potentially be used on PET-MRI for improved respiratory and cardiac motion correction.

**Keywords:** Elastic motion correction (eMOCO); positron emission tomography-magnetic resonance imaging (PET-MRI)

<sup>^</sup> ORCID: 0000-0002-8439-9498.

Submitted Sep 23, 2022. Accepted for publication Mar 07, 2023. Published online Apr 17, 2023.

doi: 10.21037/qims-22-1017

View this article at: <https://dx.doi.org/10.21037/qims-22-1017>

## Introduction

Involuntary motion caused by breathing and heart motion are a significant source of image quality degradation in positron emission tomography (PET), and robust correction methods in routine clinical settings are under constant development. In PET imaging, such motions introduce artificial quantities of radioactive tracers in regions of interest (i.e., from image blurring) and hence, result in inaccurate quantification of the standardized uptake value (SUV) (1,2). Furthermore, for imaging of the abdomen organs such as the liver, respiratory motion can result in incomplete characterization of lesions and may limit lesion detectability (3). Both types of motions are periodic/quasiperiodic and can be addressed with appropriate tracking surrogate/controlling techniques (4). Although respiratory motion can be controlled by breath-hold strategies, it is not suitable for minutes-long PET acquisitions (5,6). The alternative strategy is respiratory tracking and gating in which hardware (7) or software (8) are normally utilized to monitor and/or predict cardiac and respiratory motion.

In hybrid imaging systems such as PET/computed tomography (PET/CT) respiratory motion correction is particularly challenging as images are collected sequentially and hence, one of the modalities, or both, are used for motion modelling and correction. For step-and-shoot mode, CT-based motion modeling techniques such as gated 4D-CT (9) and synthetic gated CT from a single frame (10,11) can be used for correction during the reconstruction of PET images. However, such techniques require longer acquisition time (12) and resulting in higher radiation dose (13), and may also suffer from increased noise (14). Noise and high dose can be addressed with a PET-data driven optical flow algorithm, by calculating an elastic transformation between two images based upon the mass conservation of total activities in the field of view (FOV) (15). In the mean time, noise was partially addressed with a continuous bed motion (CBM) whole-body PET/CT system combined with the elastic motion correction (eMOCO). With this, a clinically useful reduction in noise was achieved (16,17).

However, for hybrid PET-MRI, several successful

techniques have been introduced to generate cardiac and respiratory motion models including using pulse sequences (18-21), radio frequency (RF) signal (22), and optical tracking (23). Some of these techniques utilized e.g., 2D-multi-slice T1-weighted MRI (20), or a 3-D radial stack-of-stars spoiled gradient-echo sequence to generate a set of 3-D volumes for the respiratory cycle phases (24-26). A combination of respiratory signals from a 1D MR-navigator and PET list mode was also evaluated for respiratory motion correction for pancreatic cancer patients (27,28). Such methods, however, do not differentiate between different type of breathing (slow, fast, regular or irregular). Although these techniques may generate satisfying motion models, there is a fundamental trade-off between the potentially improved resolution and increased noise. Therefore, it is necessary to invest in more advanced methods for quantifying the organ motion with less processing time and noise.

Our aim was to (I) implement the eMOCO technique on a PET-MR system, (II) to test and compare the technique in a moving phantom in static and gated techniques to establish ground truth data and (III) to evaluate how such phantom data translate into clinical PET-MR images with different dosage and motion scenarios. For the last point we evaluated different types of liver lesions and different phases of the cardiac cycle in patients to assess the respective gating techniques in a fast moving as well as slow moving environment.

## Methods

### *Phantom measurements*

All phantom and *in-vivo* image acquisitions in this study were performed on a 3.0T PET-MRI system (Biograph mMR Software Version VE11P, Siemens Healthineers, Erlangen, Germany).

A Zeus MRgRT motion management QA phantom (CIRS, Norfolk, VA) was used to perform the 4D PET-MRI measurements—see *Figure 1*. The phantom consists of a fixed body that has a central opening to allow a cylindrical insert to translate and rotate, relative to its axis to generate multidimensional motion. The motion actuator consists of

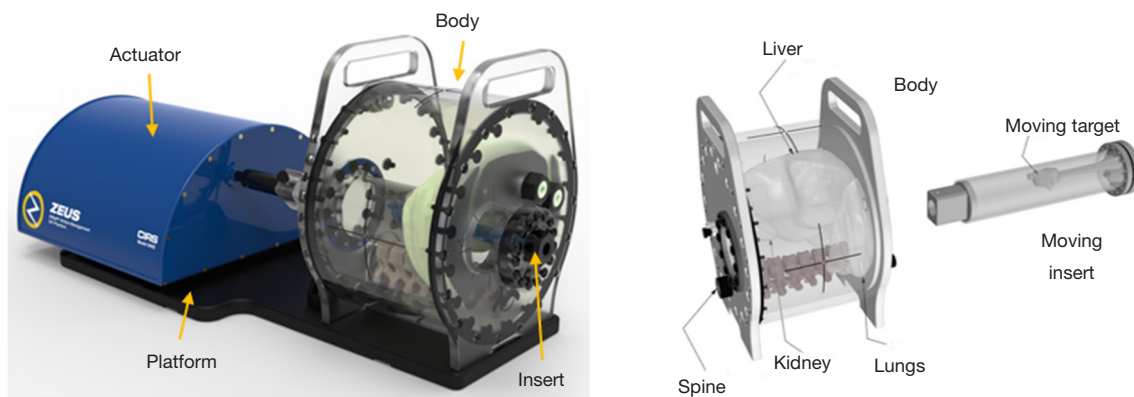


**Figure 1** 4D phantom used for acquiring the 4D PET-MRI data: phantom ensemble including the main body sub-component, a movable cylindrical insert, piston and supporting platform. PET, positron emission tomography; MRI, magnetic resonance imaging.

two piezoelectric motors and electronics encased in a non-ferromagnetic housing free of RF noise when operated. The motion is applied via a rigid piston to the cylindrical insert. The 4D phantom comes with an application software which allows the user to program the motion with a pre-defined waveform selected from a library or to import a user-defined trace.

### *Phantom preparation*

The phantom's insert and its compartment can be filled with materials to provide MR and/or PET imaging contrast. For the study presented here, the cylindrical insert container is considered as hot lesion (surrounding), whereas the tracking target compartment (0.25 mL volume) represents a cold lesion. The insert was filled with two  $^{18}\text{F}$ -FDG concentrations of 45.2 and 11.2 MBq, to simulate normal dose and low dose imaging respectively.

### *Phantom PET acquisition*

Two breathing rates (16 and 30 breath/min, to simulate normal breathing *vs.* accelerated breathing) were selected to examine the response of the technique to different breathing rates. The waveform selected from the software followed a cosine function with motion extended for approximately 12 mm. A total of four PET data sets were acquired, each for 5 min. Two sets were acquired with a normal dose scenario—at the normal and the accelerated breathing rates, while the other two data sets were evaluated as a low-dose scenario at each breathing rate.

### *Phantom data processing/reconstruction*

All PET data were normalized and corrected for attenuation, scatter, dead-time, and decay time. The full activity phantom derived PET data were considered as static, and used to compare the gated and eMOCO data. All PET images were reconstructed using ordinary Poisson ordered-subsets expectation maximization (OP-OSEM) (29) with 3 iterations and 21 subsets using a Gaussian post filter with full width at half-maximum (FWHM) of 4 mm, matrix size =  $172 \times 172$ , and zoom = 1. All reconstructions were performed using the e7-toolbox (Siemens Molecular Imaging, Knoxville, USA) (30), and for the analysis a  $0.20 \text{ cm}^3$  spherical volume of interest was selected at both, the cold and hot lesions. The signal-to-noise ratio (SNR) and contrast-to-noise ratio (CNR) for each breathing rate and dose concentration were calculated within the selected volumes-of-interest (VOIs) according to the formulas reported in (31).

### *Patient measurements*

Overall, 24 patients with dedicated PET-MR liver imaging were evaluated. Evaluation of background liver parenchyma, cold as well as hot liver lesions was derived from this data set. Also, background lung measurements were evaluated in these patients. Additionally, nine patients with dedicated cardiac PET-MRI were evaluated. This study was conducted in accordance with the Declaration of Helsinki (as revised in 2013). The study was approved by the University Health Network Review Board (No. REB-ID 16-6123 and 17-6065). Informed consent was obtained from patients

involved in this study. All patients underwent PET-MR for different study purposes and not solely for the purpose of motion correction evaluation.

### *Patient PET-MR acquisition*

Patients underwent PET-MR scans 60 minutes after the administration of  $^{18}\text{F}$ -FDG, with mean injected activity of  $4.8 \pm 0.5$  MBq/kg. This was followed by simultaneous PET-MRI scan of the abdomen and lung where PET scan duration was 10 min. An ANZAI pressure belt (ANZAI Medical Co., Ltd., Tokyo, Japan) was attached to the patient's waist to track respiratory phase and amplitude, while the cardiac cycle was tracked via electrocardiograph (ECG). The gating was determined based on the respiratory amplitude since target volume in images is often larger and more accurate compared with phase-based gating, and the differences are clinically significant, specifically for lung tumor.

MRAC was performed using the vendor's standard 2-point Dixon (3D dual-echo spoiled gradient sequence) for all patients. Other study specific sequences which were acquired for the patient studies were not further evaluated for this trial.

### *Patient data processing/reconstruction*

Similar to the phantom study, all PET images were reconstructed utilizing OP-OSEM. The full activity at maximum expiration was used as static data and compared to the motion correction techniques. For patient image reconstruction and in order to evaluate the performance of the eMOCO and gated techniques with respiratory (RG), cardiac (CG) or dual (DG) gating modes, reconstructions were performed on the same PET data set and binning of the data was performed according to the desired gating mode. This resulted into three corrected PET image sets (representing three gating modes) for each correction technique that allowed observation of the effect of each gating mode and correction technique independently.

### *Gated correction*

The gated correction was performed by retrospectively binning the PET data with the aid of physiological triggers, the ANZAI belt (for tracking the respiratory motion), and ECG (for tracking the cardiac cycle). The motion tracking signal could therefore be used independently or jointly for

binning to investigate the effect of the gating modes (CG, RG or DG) on the correction technique. The bin timing for respiratory and cardiac gating was on average of a 43 and 13 ms, respectively.

### *eMOCO correction*

The implementation of the eMOCO for the PET-MR required edits to java scripts, batch files, sinogram headers, parameter xmls, cvs spreadsheets, etc., all within the Siemens framework. The signal from the respiratory belt was used to determine the sinogram of the optimally gated frame. Then, all of the coincident events were matched to this "motion-frozen" gated frame, using the mass preservation optical flow method within the iterative motion correction reconstruction. The eMOCO algorithm was implemented in the e7-toolbox and was used to correct the PET-data in phantom as well as patient data retrospectively. The technique uses an uncorrected gated image (reference frame) and the full activity ungated blurred image (static) to calculate the motion blurring information (in the x, y and z projections), and hence a single deblurring kernel can be generated (17). The calculated deblurring kernel is used to generate a blurred image which is then forward projected and transposed to correct for motion. The technique utilizes the concept of mass preservation approach which is based on the mass preservation optical flow and independent from the motion vectors corresponding to detectable physical motion.

For the purpose of reporting, hot as well as cold liver lesions were evaluated, and the normal liver was considered as the background. Predefined spheres (1, 2 and 3  $\text{cm}^3$ ), acting as VOIs, were selected for measurements in liver, lung, left ventricle wall (LVW), apex, septum and left ventricle cavity. Different cardiac cycles (1 systole, 8 diastole and 4 in between) were chosen to perform the quantitative measurements to evaluate the effect of the cardiac cycle on the motion correction efficiency. The mean and standard deviation of the SUV at the VOIs were measured for each motion-correction technique and gating mode. To assess the performance of the eMOCO, measurements of the SNR and SUV for static and motion-corrected techniques were performed on PET images and compared. Additionally, two patients with visible PET-positive tumor in the liver were selected to investigate lesion characteristics for each motion correction technique. For example, tumors were delineated on the eMOCO image and then propagated to the gated and static images for comparison. Over-filling of this ROI

**Table 1** Phantom data

Dose	Breath/min	Static	Gated	eMOCO
Low	16	1.09±0.59	0.76±0.39	0.76±0.27
	30	1.12±0.62	1.05±0.34	0.90±0.32
High	16	4.79±1.67	3.52±1.60	3.13±0.92
	30	5.07±2.34	4.87±3.29	4.03±2.17

SUV mean  $\pm$  SD of region selected at the phantom cold lesion, and measured from motion-corrected PET images utilizing gated, and eMOCO techniques at 16 and 30 breathing rates. The measurements were performed for low and high doses. SUV, standardized uptake value; SD, standard deviation; PET, positron emission tomography; eMOCO, elastic motion correction.

at the compared images would indicate more detectable volume, and underfilling would indicate the contrary. To examine the sharpness of the image, line profiles of the tumor ROI were plotted in the anterior-posterior and left-right planes for each motion correction technique.

### Statistical analysis

The SUV mean and SD were analysed for static case as well as the motion-correction techniques, gated, and eMOCO, at different gating modes RG, CG and DG. For this analysis, a two-way ANOVA was employed while considering gating mode and motion-correction technique as the two factors, and is followed by a post-hoc Tukey's honestly significant difference (HSD) test to identify the significance between pairs of means or SD.

## Results

### Phantom study

The mean SUV and SD measured from the phantom data at low and high doses at different breathing rate are reported in *Table 1*. The mean SUV derived from eMOCO reconstruction for both breathing rates and for both, low and high doses, were found to be lower than the mean SUV measured in static images, as seen in *Figure 2A*. The respective SDs for these measurements are seen in *Table 1*. The eMOCO provided lowest SD in all settings. Measurements of SNR in the cold lesion of the phantom are demonstrated in *Figure 2B*. Here, the SNR of eMOCO was found to be less than the SNR of the static measurement. *Figure 2C* shows the CNR vs the background

noise performance for low and high doses at different breathing rates (16 and 30 b/m). For the high dose and high breathing rate, the high CNR and background noise are reported for all three techniques. The ratio between low/high dose concentration, within the phantom was found to be comparable to the ratios between low/high counts in all correction techniques (*Table 2*).

### Patient studies

Background measurements from 552 lower right lung, 458 middle right lung and 493 superior right lung (*Figure 3*) were analysed for static, gated and eMOCO reconstructions. Similarly for the liver, 1,303 liver segments were used for background SUV measurements and analyses and overall, 9 hot (FDG avid) liver lesions and 24 cold liver lesions were measured. For the heart, 386 septum regions and 392 LVW regions were used in the analysis. The global mean SUV (summarizing all measured ROI's) and SD measured from the selected regions for static and motion correction techniques in each gating mode are reported in *Table 3*.

The global mean SUV for lung and liver background measurements showed that the performance for gated and eMOCO reconstruction are comparable or improved by the eMOCO reconstruction.

### Liver measurements

The SNR measured in cold lesions and hot background are shown in (*Figure 4A*), where the SNR produced by gated techniques were significantly lower ( $P=0.012$ ) than those produced from images reconstructed using eMOCO technique. The SNR measured at the cold lesion for patients' data followed a similar pattern to the SNR measured in the phantom's cold lesion (*Figure 2B*). The CNR is also shown in *Figure 4B*, where the eMOCO produced slightly higher CNR than the gated technique. The percentage of background noise for the eMOCO is found to be lower than in the gated technique, as shown in *Figure 4C*.

The two-factor ANOVA analysis of the mean SUV's shows no statistically significant differences between motion correction techniques and the static reconstruction (*Table 4*). There was also no statistical interaction/dependency between the type of gating and the applied motion correction technique. However, again for SDs there were significant differences found (*Table 4*). Furthermore, an interaction/dependency between type of gating and technique of motion-correction was found [*Table 4*,



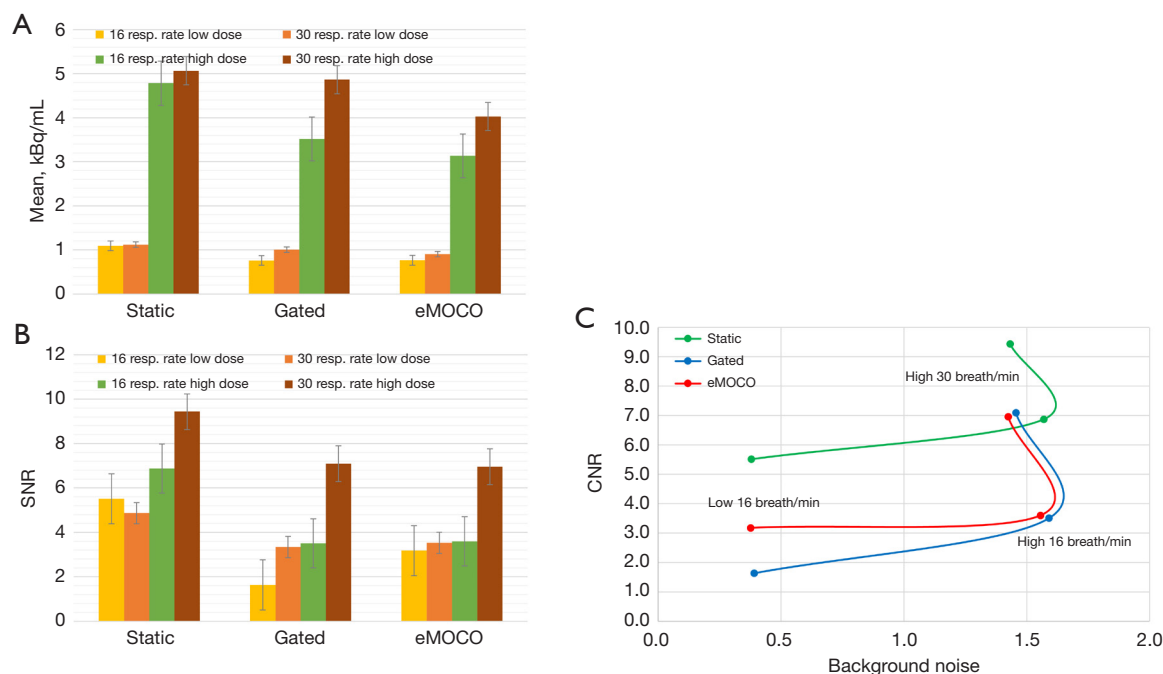


**Figure 2** Comparison of mean activities, SNR and CNR measured in the phantom for low and high doses at respiration rates of 16 and 30 breaths/min. (A) The mean activities within the cold lesion of the phantom from motion-corrected images using gated and eMOCO techniques. The mean values from low-dose measurements with 16 and 30 breaths/min are comparable between gated and eMOCO techniques. For high-dose measurements, the mean activities are also comparable between gated and eMOCO, with eMOCO showing the lowest values. (B) The SNR measured in the cold lesion of the phantom. (C) The CNR vs. background noise performance is illustrated for low and high doses and respiratory rate of 16 and 30 breaths/min. eMOCO, elastic motion correction; SNR, signal-to-noise ratio; CNR, contrast-to-noise ratio.

**Table 2** Phantom data for ratios of recovered activities

Low-to-high dose concentration ratio	Breath/min	Low-to-high counts ratio		
		Static	Gated	eMOCO
0.248	16	0.228	0.216	0.244
	30	0.221	0.207	0.225

Low/high ratio concentration of the phantom and for counts measured for each motion correction technique at both simulated breathing rates. The counts ratio for elastic motion correction eMOCO at 16 breath/min is matching the concentration ratio. eMOCO, elastic motion correction.

F(4,162) = 42.96,  $P < 0.01$ ]. Although the mean SUV for eMOCO was comparable to gated reconstruction, the SD was significantly lower ( $P < 0.05$ ) compared to the gated technique when cardiac and dual gating modes are used. They are however not statistically significantly different when using respiratory gating.

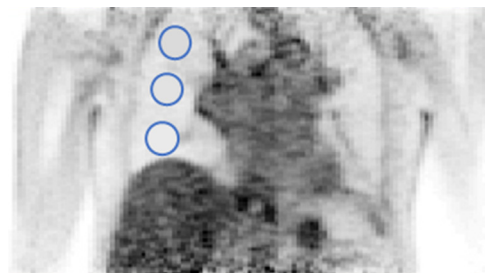


**Figure 3** Example PET image of the chest and abdomen showing three blue circled regions of interest (superior, middle, and inferior) in the lung. PET, positron emission tomography.

Figure 5A shows example images for lung and liver background for static as well as both, the gated and eMOCO reconstruction techniques. It is apparent that noise from eMOCO image is lower than the static and gated images.

For tumor characteristics, tumor detectability and delineation have improved in eMOCO by approximately

**Table 3** *In-vivo* measurements for different region of interests

Technique/region	Patients, n	ROIs, n	RG	CG	DG
<b>Static</b>					
Liver	24	1,303	2.09±0.18	–	–
Lung	24	1,503	0.44±0.10	–	–
Septum	9	386	8.86±0.56	–	–
LVW	9	392	12.92±1.63	–	–
<b>Gated</b>					
Liver			2.18±0.30	2.30±0.61	2.28±0.99
Lung			0.47±0.12	0.48±0.17	0.48±0.27
Septum			8.02±1.22	9.04±1.34	9.96±2.08
LVW			13.58±0.93	13.23±1.85	13.47±1.55
<b>eMOCO</b>					
Liver			2.17±0.23	2.20±0.31	2.12±0.39
Lung			0.46±0.09	0.47±0.10	0.47±0.10
Septum			8.36±1.00	9.16±1.20	9.68±1.16
LVW			14.70±1.27	13.88±2.20	14.58±1.52

SUV global mean ± SD of regions selected in liver, lung, septum and left ventricle wall and measured from motion-corrected PET images utilizing gated, and eMOCO techniques. An equivalent mean or lower SD is shown for eMOCO compared to the gated reconstruction throughout different gating modes (respiratory, cardiac and dual gating). SUV, standardized uptake value; SD, standard deviation; ROIs, regions of interest; LVW, left ventricle wall; PET, positron emission tomography; eMOCO, elastic motion correction; RG, respiratory gating; CG, cardiac gating; DG, dual gating.

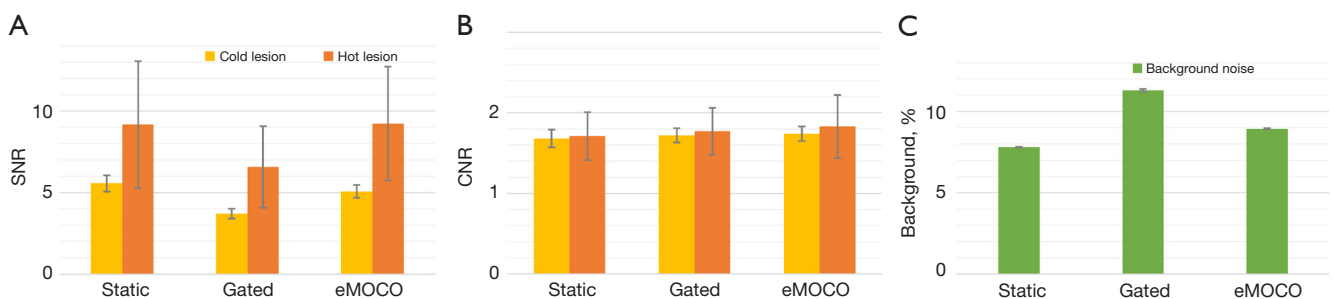


**Figure 4** Comparison SNR, CNR, and background percentage measured in patient images corrected with gated and eMOCO techniques for cold and hot lesions. (A) The mean SNR and (B) the mean CNR from motion corrected PET data using gated and eMOCO techniques for 5 hot and 7 cold lesions (patients), are shown. The percentages of background noise (solid green bars) for all reconstruction techniques are also shown in (C). Percentage noise from the eMOCO images were found to be lower, compared to the gated technique. PET, positron emission tomography; SNR, signal-to-noise ratio; CNR, contrast-to-noise ratio; eMOCO, elastic motion correction.

**Table 4** Two-way analysis of variance results

Factor	Liver	Lung	Heart
Mean SUV			
Gating mode	[F(2,162) =0.17, P=0.84]	[F(2,162) =930.90, P<0.01]	[F(2,216) =86.99, P<0.01]
Motion-correction techniques	[F(2,162) =0.12, P=0.89]	[F(2,162) =0.83, P=0.44]	[F(2,216) =87.55, P<0.01]
Interaction	[F(4,162) =0.40, P=0.81]	[F(4,162) =2.28, P=0.06]	[F(4,216) =14.00, P<0.01]
SD			
Gating mode	[F(2,162) =60.41, P<0.01]	[F(2,162) =28.371, P<0.01]	[F(2,216) =155.75, P<0.01]
Motion-correction techniques	[F(2,162) =180.61, P<0.01]	[F(2,162) =56.51, P<0.01]	[F(2,216) =162.62, P<0.01]
Interaction	[F(4,162) =42.96, P<0.01]	[F(4,162) =13.68, P<0.01]	[F(4,216) =36.38, P<0.01]

Two-factor ANOVA testing results of motion-correction techniques and gating modes in liver, lung and heart measurements. The SUV mean and SD at the heart are showing partly significant differences and dependency between the gating mode and the motion-correction technique. ANOVA, analysis of variance; SUV, standardized uptake value; SD, standard deviation.

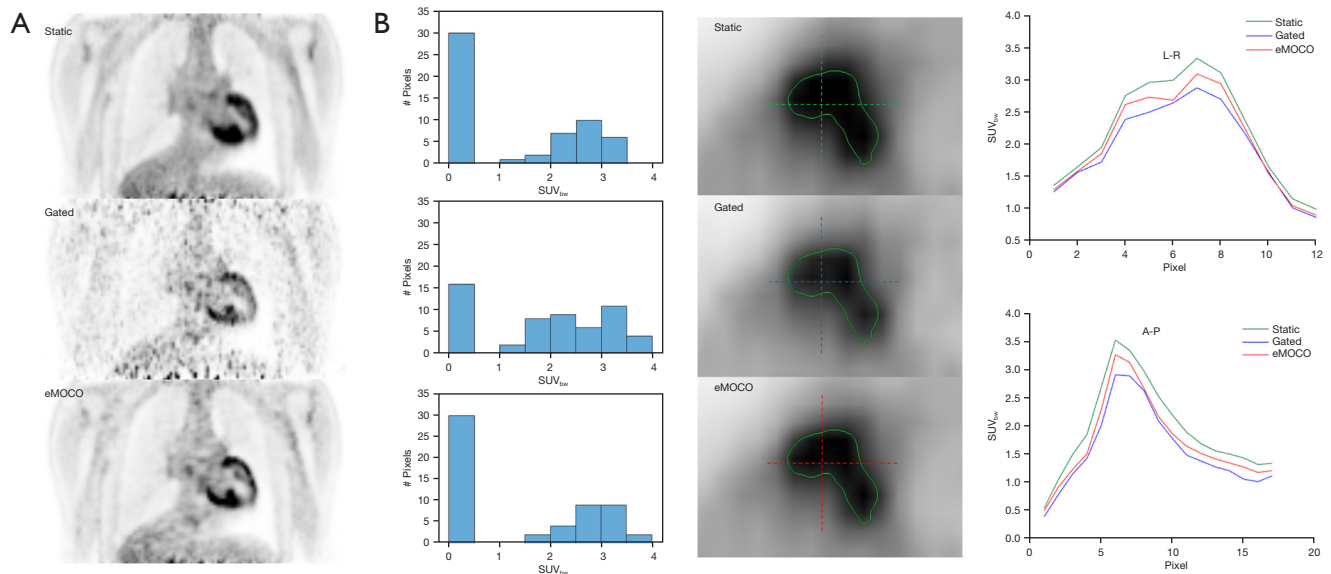


**Figure 5** Comparison of a sample patient's images that are motion-corrected with different techniques, and their effects on tumor characterization. (A) coronal view for cardiac motion-corrected images, from top to bottom, are the static, gated and eMOCO, respectively. (B) The results from the analysis of the liver tumor are shown, including from left to right, the histograms of the activity distribution in the tumor, the tumor images and the line profiles across the tumor, in the left-right (L-R) and anterior-posterior (A-P) directions. eMOCO, elastic motion correction; SUV, standardized uptake value.

4% over the gated reconstruction (*Figure 5B*). On eMOCO reconstructed images, sharper edges can be observed from the steeper line profile, as seen in *Figure 5B*.

### Lung measurements

A sample of patient-derived lung PET images produced

by the static, gated and eMOCO techniques are shown in *Figure 6*—here, the noise level in the eMOCO reconstruction is shown to be lower than the gated images. The mean SUV were found not to be statistically significant different between static, gated and eMOCO, while the two-way ANOVA test shows significant differences [see *Table 4*,  $F(2,162) =930.9$ ,  $P<0.01$ ] in the mean SUV (when applying



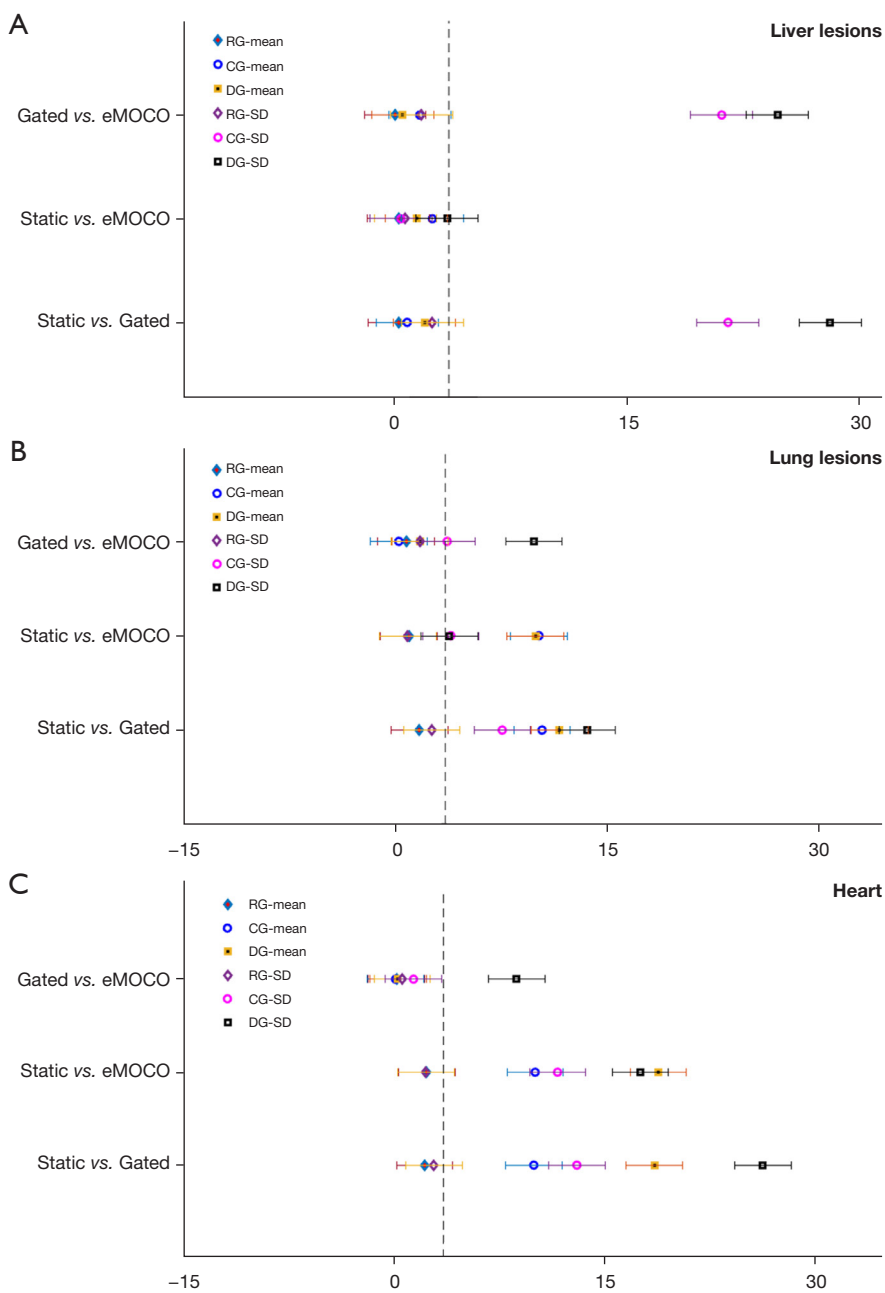


**Figure 6** A display of post-hoc Tukey's HSD Q-statistic results with 3.408 as the cut-off (vertical dashed line) between significant ( $Q > 3.408$ ) and not significant ( $Q < 3.408$ ) differences. The HSD representing the significant differences between the mean SUV, and also the SD, for a pair of reconstruction techniques at different gating modes, respiratory-gating (RG-mean and RG-SD), cardiac-gating (CG-mean and CG-SD), dual-gating (DG-mean and DG-SD), for the regions of the (A) liver, (B) lung and (C) heart. For the liver (A), the test shows high significant difference between SD of gated and eMOCO techniques when applying either CG-SD or DG-SD modes. HSD, honestly significant difference; RG, respiratory gating; CG, cardiac gating; DG, dual gating; eMOCO, elastic motion correction; SUV, standardized uptake value; SD, standard deviation.

	Liver			Lung			Heart			Septum *		LVW **	
	RG	CG	DG	RG	CG	DG	RG	CG	DG	CG	DG	CG	DG
<b>Mean SUV</b>													
Static vs. Gated	0.900	0.816	0.357	0.471	0.001	0.001	0.284	0.001	0.001	0.007	0.015	0.536	0.476
Static vs. eMOCO	0.900	0.200	0.573	0.770	0.001	0.001	0.234	0.001	0.001	0.029	0.044	0.012	0.006
Gated vs. eMOCO	0.900	0.487	0.900	0.845	0.900	0.452	0.900	0.900	0.900	0.726	0.821	0.098	0.069
<b>SD</b>													
Static vs. Gated	0.205	0.001	0.001	0.181	0.001	0.001	0.120	0.001	0.001	0.003	0.001	0.842	0.900
Static vs. eMOCO	0.863	0.900	0.052	0.803	0.021	0.026	0.253	0.001	0.001	0.012	0.098	0.357	0.900
Gated vs. eMOCO	0.441	0.001	0.001	0.463	0.034	0.001	0.900	0.590	0.001	0.724	0.011	0.654	0.900
insignificant	P<0.05	P<0.01	* Indicates phase (4) in-between systole and diastole, while ** indicates systole phase (1)										

**Figure 7** Statistical results for Tukey test. Post-hoc Tukey test results (P values) of measured mean SUV in liver, lung and heart images, which were reconstructed with different motion correction techniques and gating modes. RG, respiratory gating; CG, cardiac gating; DG, dual gating; eMOCO, elastic motion correction; SUV, Standardized uptake value; SD, standard deviation; LVW, left ventricle wall.

different gating modes). Similar to the liver results, the two-way ANOVA test on the SD showed significant differences between the motion-correction techniques [Table 4,  $F(2,162) = 56.51$ ,  $P < 0.01$ ], as well as the gating modes [Table 4,  $F(2,162) = 28.37$ ,  $P < 0.01$ ].

### Heart measurements

Overall, mean SUV and SD measured in the heart VOI's reconstructed with eMOCO, gated and static were statistically significantly different. There were also significance dependences in the mean SUV's of the motion-correction techniques and the gating modes (Table 4).

### Post-hoc Tukey's HSD testing

The results from the post-hoc Tukey's HSD with studentized range statistic (Q-statistic) for liver, lung and heart measurements are shown in Figure 6A-6C respectively, the corresponding HSD P values are shown in Figure 7. The most significant differences of the mean SUV and SD are seen in static vs. gated reconstruction ( $P < 0.01$ ) and gated reconstruction vs. eMOCO ( $P < 0.01$ ) when CG or DG techniques are applied.

The post-hoc Tukey's HSD test showed that the mean SUV for static vs. gated reconstruction and static vs. eMOCO reconstruction are significantly different when using cardiac gating in lung and heart measurements ( $P < 0.01$ ), while this is not the case for gated vs. eMOCO as seen in Figure 7.

### Discussion

Although elastic motion correction (eMOCO) is usually used in PET/CT to correct for cardiac and respiratory motions in PET images (30,32,33), the eMOCO technique has not been implemented and tested in a PET-MR environment.

In this study, we implemented the eMOCO technique for the PET-MRI system, which required specific modifications of the eMOCO scripts to suit the PET-MR setting. The scope was however not only to implement the eMOCO into a PET-MR system, but also compare its performance to similar PET-based motion corrections in a moving phantom to establish a ground truth, as well as, test the transferability of the phantom data results to clinical patient data.

The main finding from the analysis is that the eMOCO improved the SD in different reconstructions and thereby provided lower noise levels within the images. The phantom results suggest that eMOCO would not necessarily improve the SNR in cold lesions. However, it may still improve detectability since the SNR at cold lesion is not necessarily correlated to detection performance as it is with hot lesions.

The statistical analysis of the hot lesions within the liver presented no significant differences between the mean SUV, however the SD from eMOCO images was found to be statistically significantly lower when compared with the gated techniques. This indicates that the eMOCO enables PET-images with less statistical noise compared to the standard clinical gating technique. The lower SD in images corrected by eMOCO was apparent in liver, lung and heart

VOIs measurements and in particular when cardiac and dual gating was applied. This suggests a dependency of the cardiac and dual gating modes on the correction technique. One explanation is that the eMOCO algorithm, when applied to all phases of the cardiac cycle (8 phases), includes the counts of all cardiac gates into the reference gate (30).

From a clinical/practical perspective, the here found advantages of the eMOCO might not be as impressive as initially anticipated or as good as PET/CT, at least not within our group. Therefore, it is worth mentioning that images corrected by eMOCO on a PET/CT scanner benefit from the time-of-flight (TOF) feature, which increases SUV<sub>max</sub>, SUV<sub>mean</sub>, and SNR. In our study, the mMR-Biograph does not use TOF, and so the eMOCO results might not be as impressive as the results of eMOCO on PET/CT. However, the specific improvements which have been found are nevertheless important for clinical reading. First of all, the fact that the results from the phantom measurements are translated into patient imaging findings speaks for the robustness of the method. The results, namely the reduced noise/increased SNR are important for clinical reading as it provides the radiologist/imaging reader with increased accuracy for quantification. This is especially important in follow-up studies where clinical decisions are dependent of accurate measurement of differences or quantification of lesions. Many therapy decision criteria are now based on measurement of ratio's (i.e., Deauville Criteria for lymphoma or myeloma, Hopkins Criteria for Head and Neck cancer, PROMISE score for PSMA imaging or Krenning Score for neuroendocrine tumour imaging). The increased consistency and reduction of standard deviation provided by the eMOCO compared to other reconstruction methods is offering additional accuracy for those specific clinical scenarios.

There are several strategies to achieve PET-based motion compensation within PET-MRI. The core requirement for a given strategy is an accurate respiratory motion model that can be generated with either the aid of external device (i.e., belt), MR data or PET data. Common MR-based respiratory motion models such as retrospective gating and averaging over multiple respiratory cycles (34) usually provide better image quality but are unable to reflect inter-cycle variations in the respiration pattern. Another MR-based motion model can be generated using fast MR pulse sequences, but images may suffer loss of SNR and decreased spatial resolution. While MR-based MOCO techniques can be applied to PET data using either motion compensated image reconstruction (MCIR) (34) or

post-reconstruction registration (PRR) (35), they usually require specific modified pulse sequence in place, and/or performing MRI scanning throughout the whole PET acquisition time. One example of these techniques is the BodyCompass<sup>TM</sup> (36-38) which utilizes a 3D T1-weighted radial stack-of-stars MRI pulse sequence to calculate the respiratory signal and create the motion model. In this sequence, the respiratory signal is acquired during the full PET acquisition in order to preserve both high spatial resolution and the different respiratory patterns. The technique does not require a navigator echo or external devices as a source of motion signal, instead, self-gating in a retrospective PRR reconstruction fashion is utilized. The drawback of this technique is the need for optimization of number of bins and bin sizes which are required to reduce the intra-bin motion at the diaphragm. Additionally, to generate a sufficient motion model in this case, relatively long scan time is also required which subsequently may thwarts useful MRI information during this time. It is worth mentioning here that BodyCompass was not reported in this study, since it could not be implemented with phantom acquisitions.

In contrast to self-gated MR-based MOCO, PET-based eMOCO, reported in this study, depends only on the sensor that provides the motion information while utilizing the PET data itself without the dependency on inputs from the MR side. This allowed the use of the PET-data fully without the loss of information from both MRI and PET modalities. The eMOCO algorithm computation time was also tolerable to a clinical setting which is an advantage in terms of the complete reconstruction time. Other PET-based motion correction technique recently proposed are for example data driven motion correction techniques (DDMC), i.e., for cardiac motion correction (39). Here the authors binned the position of the positron annihilation events rather than the line of response (LOR) and reported accurate cardiac motion correction. However, this required the aid of TOF to achieve improved results and it was incorporated without adjustments for normalization, scatter, or randoms correction. Overall CNR produced by the eMOCO is moderately significantly better in phantom measurements than the gated technique, in breathing type motion corrections, even with lower doses—overall offering several advantages for those type of acquisitions. This was found to be even true for cardiac imaging.

The decision on which technique to be used for motion correction still depends on the availability of the algorithms used in motion model generation and

correction, as well as the scanner time. In our study we were able to perform the eMOCO technique with the aid of offline reconstruction eMOCO combined algorithm which required specific settings which are not yet available for clinical routine. Nevertheless, the proposed eMOCO requires less computational time, and can be a valuable choice to use with PET-MR. Finally, this work opens the door for future research, for example by using the motion blurring information from PET as a quality assurance for motion compensation in MR. This concept appears possible considering that a recent study combined both, the motion information from both modalities which improved final motion model accuracy by 15% (40).

Our study has certain limitations. One possible limitation is that we did not compare the eMOCO to advanced PET-based motion correction techniques. However, comparison was limited to the gated technique, since we wanted to show the capability of this specific method, and transferability of the results from the phantom measurements into clinical imaging. Additionally, the phantom experiment could have benefitted from including the MR-based BodyCompass for comparison. This is possible if the appropriate signal feed from the phantom to the scanner is available for implementation, which was not the case at the time of this experiment.

Although ANZAI belt is used frequently in PET/CT scans to provide the respiratory signal, some failure to provide adequate signal was frequently reported, and hence the high noise results we have from the gated technique could be affected. We evaluated a limited number of patients with biopsy confirmed tumor, and therefore, the tumor detectability results we report here might be of statistically limited value.

While the underlying technological principle of eMOCO is certainly similar in PET/CT and PET-MR, the integration into a different hybrid and simultaneous imaging modality contains novel information to our opinion. Integration into a different hybrid modality is not straightforward, needs a significant amount of alterations/adaption for integration and needs testing, to be accepted for clinical applications,

## Conclusions

In conclusion, the elastic motion correction technique partly significantly reduced SD in PET measurements and thereby reduced noise compared to the static and gated datasets. Thus, overall improved quantification of lesions

can be enabled by this technique. The eMOCO technique is a viable option for improved respiratory and cardiac motion correction method and appears to be beneficial in a clinical setting.

## Acknowledgments

*Funding:* None.

## Footnote

*Conflicts of Interest:* All authors have completed the ICMJE uniform disclosure form (available at <https://qims.amegroups.com/article/view/10.21037/qims-22-1017/coif>). JS, IH and JJ are full-time employees of Siemens Healthcare. UM reports that he received consulting fee from POINT Biopharma Inc. (2020–2022). KH reports that he received honoraria from Sanofi-genzyme. PVH reports that he received grants, support for attending meetings and WIP software from Siemens Healthineers; and he also received speaker fees from Spring Nature, JCA Seminars, and Ontario association of radiologists. The other authors have no conflicts of interest to declare.

*Ethical Statement:* The authors are accountable for all aspects of the work in ensuring that questions related to the accuracy or integrity of any part of the work are appropriately investigated and resolved. The study was conducted in accordance with the Declaration of Helsinki (as revised in 2013). The study was approved by the University Health Network Review Board (No. REB-ID 16-6123 and 17-6065). Informed consent was obtained from patients involved in this study.

*Open Access Statement:* This is an Open Access article distributed in accordance with the Creative Commons Attribution-NonCommercial-NoDerivs 4.0 International License (CC BY-NC-ND 4.0), which permits the non-commercial replication and distribution of the article with the strict proviso that no changes or edits are made and the original work is properly cited (including links to both the formal publication through the relevant DOI and the license). See: <https://creativecommons.org/licenses/by-nc-nd/4.0/>.

## References

1. Osman MM, Cohade C, Nakamoto Y, Wahl RL. Respiratory motion artifacts on PET emission images

- obtained using CT attenuation correction on PET-CT. *Eur J Nucl Med Mol Imaging* 2003;30:603-6.
2. Erdi YE, Nehmeh SA, Pan T, Pevsner A, Rosenzweig KE, Mageras G, Yorke ED, Schoder H, Hsiao W, Squire OD, Vernon P, Ashman JB, Mostafavi H, Larson SM, Humm JL. The CT motion quantitation of lung lesions and its impact on PET-measured SUVs. *J Nucl Med* 2004;45:1287-92.
  3. Li G, Schmidtlein CR, Burger IA, Ridge CA, Solomon SB, Humm JL. Assessing and accounting for the impact of respiratory motion on FDG uptake and viable volume for liver lesions in free-breathing PET using respiration-suspended PET images as reference. *Med Phys* 2014;41:091905.
  4. Gillman A, Smith J, Thomas P, Rose S, Dowson N. PET motion correction in context of integrated PET/MR: Current techniques, limitations, and future projections. *Med Phys* 2017;44:e430-45.
  5. Nagamachi S, Wakamatsu H, Kiyohara S, Fujita S, Futami S, Arita H, Nishii R, Tamura S, Kawai K. Usefulness of a deep-inspiration breath-hold 18F-FDG PET/CT technique in diagnosing liver, bile duct, and pancreas tumors. *Nucl Med Commun* 2009;30:326-32.
  6. Raper AJ, Richardson DW, Kontos HA, Patterson JL Jr. Circulatory responses to breath holding in man. *J Appl Physiol* 1967;22:201-6.
  7. Bailey DL, Kalemis A. Externally triggered gating of nuclear medicine acquisitions: a useful method for partitioning data. *Phys Med Biol* 2005;50:N55-62.
  8. Werner MK, Parker JA, Kolodny GM, English JR, Palmer MR. Respiratory gating enhances imaging of pulmonary nodules and measurement of tracer uptake in FDG PET/CT. *AJR Am J Roentgenol* 2009;193:1640-5.
  9. Pönisch F, Richter C, Just U, Enghardt W. Attenuation correction of four dimensional (4D) PET using phase-correlated 4D-computed tomography. *Phys Med Biol* 2008;53:N259-68.
  10. McQuaid SJ, Lambrou T, Hutton BF. A novel method for incorporating respiratory-matched attenuation correction in the motion correction of cardiac PET-CT studies. *Phys Med Biol* 2011;56:2903-15.
  11. Fayad H, Lamare F, Bettinardi V, Roux C, Visvikis D, editors. Respiratory synchronized CT image generation from 4D PET acquisitions. *IEEE Nuclear Science Symposium Conference Record* 2008: IEEE.
  12. Allen-Auerbach M, Yeom K, Park J, Phelps M, Czernin J. Standard PET/CT of the chest during shallow breathing is inadequate for comprehensive staging of lung cancer. *J Nucl Med* 2006;47:298-301.
  13. Nye JA, Esteves F, Votaw JR. Minimizing artifacts resulting from respiratory and cardiac motion by optimization of the transmission scan in cardiac PET/CT. *Med Phys* 2007;34:1901-6.
  14. Souvatzoglou M, Bengel F, Busch R, Kruschke C, Fernolendt H, Lee D, Schwaiger M, Nekolla SG. Attenuation correction in cardiac PET/CT with three different CT protocols: a comparison with conventional PET. *Eur J Nucl Med Mol Imaging* 2007;34:1991-2000.
  15. Dawood M, Gigengack F, Jiang X, Schafers KP. A mass conservation-based optical flow method for cardiac motion correction in 3D-PET. *Med Phys* 2013;40:012505.
  16. Hong I, Jones J, Hamill J, Michel C, Casey M, editors. Elastic motion correction for continuous bed motion whole-body PET/CT. 2016 IEEE Nuclear Science Symposium, Medical Imaging Conference and Room-Temperature Semiconductor Detector Workshop (NSS/MIC/RTSD); 2016: IEEE.
  17. Hong I, Jones J, Casey M, editors. Ultrafast elastic motion correction via motion deblurring. 2014 IEEE Nuclear Science Symposium and Medical Imaging Conference (NSS/MIC) 2014: IEEE.
  18. Munoz C, Neji R, Cruz G, Mallia A, Jeljeli S, Reader AJ, Botnar RM, Prieto C. Motion-corrected simultaneous cardiac positron emission tomography and coronary MR angiography with high acquisition efficiency. *Magn Reson Med* 2018;79:339-50.
  19. Kolbitsch C, Prieto C, Tsoumpas C, Schaeffter T. A 3D MR-acquisition scheme for nonrigid bulk motion correction in simultaneous PET-MR. *Med Phys* 2014;41:082304.
  20. Würslin C, Schmidt H, Martirosian P, Brendle C, Boss A, Schwenzer NF, Stegger L. Respiratory motion correction in oncologic PET using T1-weighted MR imaging on a simultaneous whole-body PET/MR system. *J Nucl Med* 2013;54:464-71.
  21. Robson PM, Trivieri M, Karakatsanis NA, Padilla M, Abgral R, Dweck MR, Kovacic JC, Fayad ZA. Correction of respiratory and cardiac motion in cardiac PET/MR using MR-based motion modeling. *Phys Med Biol* 2018;63:225011.
  22. Han F, Rapacchi S, Hu P. Prospective cardiac motion self-gating. *Quant Imaging Med Surg* 2017;7:215-26.
  23. Wijenayake U, Park SY. Real-Time External Respiratory Motion Measuring Technique Using an RGB-D Camera and Principal Component Analysis. *Sensors (Basel)* 2017.
  24. Grimm R, Fürst S, Dregely I, Forman C, Hutter JM,



- Ziegler SI, Nekolla S, Kiefer B, Schwaiger M, Hornegger J, Block T. Self-gated radial MRI for respiratory motion compensation on hybrid PET/MR systems. *Med Image Comput Comput Assist Interv* 2013;16:17-24.
25. Kolbitsch C, Ahlman MA, Davies-Venn C, Evers R, Hansen M, Peressutti D, Marsden P, Kellman P, Bluemke DA, Schaeffter T. Cardiac and Respiratory Motion Correction for Simultaneous Cardiac PET/MR. *J Nucl Med* 2017;58:846-52.
  26. Gratz M, Ruhlmann V, Umutlu L, Fenchel M, Hong I, Quick HH. Impact of respiratory motion correction on lesion visibility and quantification in thoracic PET/MR imaging. *PLoS One* 2020;15:e0233209.
  27. Manber R, Thielemans K, Hutton BF, Barnes A, Ourselin S, Arridge S, O'Meara C, Wan S, Atkinson D. Practical PET Respiratory Motion Correction in Clinical PET/MR. *J Nucl Med* 2015;56:890-6.
  28. Manber R, Thielemans K, Hutton BF, Wan S, Fraioli F, Barnes A, Ourselin S, Arridge S, Atkinson D. Clinical Impact of Respiratory Motion Correction in Simultaneous PET/MR, Using a Joint PET/MR Predictive Motion Model. *J Nucl Med* 2018;59:1467-73.
  29. Comtat C, Bataille F, Michel C, Jones JP, Sibomana M, Janeiro L, et al., editors. OSEM-3D reconstruction strategies for the ECAT HRRT. *IEEE Symposium Conference Record Nuclear Science* 2004.
  30. Bellinge JW, Majeed K, Carr SS, Jones J, Hong I, Francis RJ, Schultz CJ. Coronary artery 18F-NaF PET analysis with the use of an elastic motion correction software. *J Nucl Cardiol* 2020;27:952-61.
  31. Yan J, Schaefferkoette J, Conti M, Townsend D. A method to assess image quality for Low-dose PET: analysis of SNR, CNR, bias and image noise. *Cancer Imaging* 2016;16:26.
  32. Pösse S, Büther F, Mannweiler D, Hong I, Jones J, Schäfers M, Schäfers KP. Comparison of two elastic motion correction approaches for whole-body PET/CT: motion deblurring vs gate-to-gate motion correction. *EJNMMI Phys* 2020;7:19.
  33. Meier JG, Wu CC, Betancourt Cuellar SL, Truong MT, Erasmus JR, Einstein S, Mawlawi O. Evaluation of a novel elastic respiratory motion correction algorithm on quantification and image quality in abdomino-thoracic PET/CT. *J Nucl Med* 2018. [Epub ahead of print]. doi: 10.2967/jnumed.118.213884.
  34. Ouyang J, Li Q, El Fakhri G. Magnetic resonance-based motion correction for positron emission tomography imaging. *Semin Nucl Med* 2013;43:60-7.
  35. Chun SY, Reese TG, Ouyang J, Guerin B, Catana C, Zhu X, Alpert NM, El Fakhri G. MRI-based nonrigid motion correction in simultaneous PET/MRI. *J Nucl Med* 2012;53:1284-91.
  36. Grimm R, Fürst S, Souvatzoglou M, Forman C, Hutter J, Dregely I, Ziegler SI, Kiefer B, Hornegger J, Block KT, Nekolla SG. Self-gated MRI motion modeling for respiratory motion compensation in integrated PET/MRI. *Med Image Anal* 2015;19:110-20.
  37. Chen Z, Sforazzini F, Baran J, Close T, Shah NJ, Egan GF. MR-PET head motion correction based on co-registration of multicontrast MR images. *Hum Brain Mapp* 2021;42:4081-91.
  38. Fürst S, Grimm R, Hong I, Souvatzoglou M, Casey ME, Schwaiger M, Nekolla SG, Ziegler SI. Motion correction strategies for integrated PET/MR. *J Nucl Med* 2015;56:261-9.
  39. Armstrong IS, Hayden C, Memmott MJ, Arumugam P. A preliminary evaluation of a high temporal resolution data-driven motion correction algorithm for rubidium-82 on a SiPM PET-CT system. *J Nucl Cardiol* 2022;29:56-68.
  40. Mayer J, Jin Y, Wurster TH, Makowski MR, Kolbitsch C. Evaluation of synergistic image registration for motion-corrected coronary NaF-PET-MR. *Philos Trans A Math Phys Eng Sci* 2021;379:20200202.

**Cite this article as:** Farang A, Schaefferkoetter J, Kohan A, Hong I, Jones J, Stanescu T, Hanneman K, Sapisochin G, Yeung I, Metser U, Veit-Haibach P. Respiratory and cardiac motion correction in positron emission tomography using elastic motion approach for simultaneous abdomen and thorax positron emission tomography-magnetic resonance imaging. *Quant Imaging Med Surg* 2023;13(5):3185-3198. doi: 10.21037/qims-22-1017